
**Climb of jogs as a rate-limiting process of screw dislocation motion in olivine
dislocation creep**

Lin Wang^{a, b} and Tomoo Katsura^{a, c}

^a Bayerisches Geoinstitut, University of Bayreuth, 95440 Bayreuth, Germany.

^b Geophysical laboratory, Carnegie institution for Science, Washington D.C., 20015, U.S.A.

^c Center for High Pressure Science and Technology Advanced Research, Beijing, 100094, China

* Corresponding author.

E-mail address: liwang@carnegiescience.edu

11 **Abstract**

12 Dislocation recovery experiments were conducted on predeformed olivine single crystals at
13 temperatures of 1,450 to 1,760 K, room pressure, and oxygen partial pressures near the Ni-NiO
14 buffer to determine the annihilation rate constants for [001](010) edge dislocations. The obtained
15 rate constants were found to be comparable to those of previously determined [001] screw
16 dislocations. The activation energies for the motion of both dislocations are identical. This result
17 suggests that the motion of screw dislocations in olivine is not controlled by cross-slip but by the
18 same rate-limiting process of the motion of edge dislocations, i.e., climb, under low-stress,
19 high-temperature conditions. The diffusivity derived from dislocation climb indicates that
20 dislocation recovery is controlled by Si pipe diffusion, rather than Si lattice diffusion. Our results
21 suggest that the conventional climb-controlled model for olivine can be applied to motions of not
22 only edge but also screw dislocations. Therefore, the previous proposed cross-slip model cannot
23 explain the softness of asthenosphere.

24
25 **Keywords:** dislocation recovery, dislocation creep, temperature dependence, climb controlled
26 model, asthenosphere

28 **Introduction**

29 Geophysical observations regarding geoid (e.g., Hager, 1991) and postglacial rebound (e.g.,
30 Peltier, 1998) have suggested that a soft asthenosphere underlies a rigid lithosphere. Geodynamic
31 modeling (e.g., Becker, 2017; Craig and McKenzie, 1986) have also suggested the same conclusion.
32 The reason for the presence of soft asthenosphere is under debate. Although the simplest
33 explanation cites a weakening of materials due to high temperatures, the results of deformation

34 experiments conducted on dry peridotite implied that high temperatures are insufficient to explain
35 the softness of the asthenosphere (Hirth and Kohlstedt, 2003). A popular explanation refers to the
36 hydrous weakening of olivine (e.g., Mackwell et al., 1985; Hirth and Kohlstedt, 2003). However
37 this has been refuted by recent Si self-diffusion experiments (Fei et al., 2016; Fei et al., 2013) based
38 on the assumption that dislocation creep is controlled by diffusion. Another possible explanation
39 was proposed by Poirier and Vergobbi (1978). The authors suggested that if the cross-slip of
40 dissociated screw dislocations controls olivine dislocation creep, the estimated upper-mantle
41 viscosity would be one order of magnitude lower than that predicted by the climb-controlled model
42 in a stress range from 10 to 100 bar. This property may explain the softness of the asthenosphere.
43 However, no experimental study has tested this hypothesis.

44 Neither diffusion nor deformation experiments can identify the rate-limiting process of
45 motions of screw dislocations. Diffusion does not involve motions of dislocations. Although it is
46 theoretically possible to determine the rate-limiting process of dislocation motions by examining the
47 stress dependence of creep rates (e.g., Hirth and Kohlstedt, 2003), the stress ranges applied in
48 deformation experiments are too narrow. The conventionally used stress exponent of 3.5 for
49 dislocation creep implies a pipe diffusion-controlled mechanism (Hirth and Kohlstedt, 2003, 2015).
50 However, such experiments have a stress range only from 100 to 224 MPa. On the other hand,
51 Kohlstedt and Goetze (1974) found that the stress exponent increases with increasing stress. Poirier
52 (1985, P.139) found that the stress exponent of olivine single crystal dislocation creep varies from
53 2.6 to 3.7 in different studies.

54 In the present study, we conducted dislocation recovery experiments on [001](010) edge
55 dislocations and compared the results with those of [001](010) screw dislocations given by Wang et

al. (2016). During recovery, dislocations move on (glide) and out of the slip plane (climb, cross-slip) successively under the influence of internal stress. Therefore, the activation energy determined by this method represents that of the rate-limiting process of dislocation motions. Although the model developed by Poirier and Vergobbi (1978) was based on [100] screw dislocations, the important point in their model is the dissociation, rather than Burgers vector of dislocations. Because dissociation of [001] screw dislocations have been confirmed in olivine (Vander Sande and Kohlstedt, 1976), [001] screw dislocation can be used to test this hypothesis. In addition, most of [100] dislocations have an edge character at temperatures of less than 1350 °C (Bai and Kohlstedt, 1992; Wang et al., 2016). while [001] dislocations has similar density of edge and screw components (Wang et al., 2016). This indicates the equivalent importance of both types of dislocations in this slip system. Therefore, we focus on the [001](010) slip system in this study (hereafter called *c*-dislocations).

Experimental Procedure

The same Pakistan olivine and sample preparation procedures as those of Wang et al. (2016) were employed in this study. The composition of olivine was reported by Gose et al. (2010). The experimental setup used is similar to that used in Wang et al. (2016). The olivine single crystal was oriented by X-ray diffraction and electron backscattered diffraction (EBSD) and then placed in the cell assembly such that the [001] direction and (010) plane were parallel to the shear direction and plane, respectively.

Dislocations with the [001] Burgers vector on the (010) plane were produced by experimental deformation using a Kawai-type multianvil apparatus at the University of Bayreuth. The sample

78 assembly was first pressurized to 3 GPa with a press load of 3.6 MN and then heated to a
79 temperature of 1,600 K and held for 15 min to sinter crushable alumina. After this, the assembly
80 was further compressed to a press load of 3.9 MN for 15 min to deform the sample. After
81 deformation, the sample was quenched by switching off the heating power and then decompressed
82 to room pressure for more than 16 hours. Transmission electronic microscopy (TEM) results
83 presented by Wang et al. (2016) found the [001](010) slip system to be successfully activated and
84 dominant using this procedure. The ratio of screw to edge dislocations was 3:2 as reported by Wang
85 et al. (2016).

86 The deformed olivine crystals were cut into eight cubic pieces and paired into four groups, in
87 which the two pieces in each group shared a common (100) plane. One piece from each pair was
88 used to determine the initial dislocation density while the other was used to determine dislocation
89 density after annealing. The annealing experiments were conducted at ambient pressure and
90 temperatures of 1,460 to 1,760 K for 35 min to 24 hours using a gas mixing furnace. The oxygen
91 partial pressure was controlled at 10^{-6} - 10^{-8} MPa, which is near the Ni-NiO buffer, using a CO-CO₂
92 gas mixture. Table 1 summarizes the conditions of the annealing experiments.

93 Dislocations were observed using the oxidation decoration technique (Kohlstedt et al., 1976,
94 Karato 1987). Corresponding areas away from subgrain boundaries on the common (100) plane in
95 initial and annealed pieces of the same group were observed to determine the change in dislocation
96 screw lattice friction in the [001](010) slip system makes the screw and edge components nearly
97 straight in this slip system (Bai and Kohlstedt 1992, sample deformed in [011]_c orientation, Wang et
98 al., 2016, *c*-deformed sample). This enable us to distinguish the characters of dislocations by using
99 line geometry of dislocations (Ogawa and Karato, 1989). Since [001](010) edge dislocations

100 elongate in the [100] direction, these dislocations show dots contrasted on the (100) plane in
101 backscattered images after decoration. The number of dots per unit area was counted as the
102 dislocation density.

103 Annihilation rate constants were calculated via second-order dislocation recovery kinetics
104 (Karato and Ogawa, 1982; Kohlstedt et al., 1980; Wang et al., 2016)

$$105 \quad k = \frac{\frac{1}{\rho_f} - \frac{1}{\rho_i}}{t}, \quad (2)$$

106 where ρ_f and ρ_i are the dislocation densities after and before annealing, respectively, and t is the
107 annealing time. Due to the thermally activated process, the dislocation annihilation rate constant is
108 assumed to follow the Arrhenius relationship:

$$109 \quad k = k_0 \exp\left(-\frac{E}{RT}\right) \quad (3)$$

110 where k_0 is a constant, E is the activation energy of dislocation annihilation, T is temperature, and
111 R is the gas constant.

112

113 **Results**

114 Table 1 shows experimental results together with the annealing conditions. Dislocation density
115 in the samples before deformation is less than $0.0004 \mu\text{m}^{-2}$, which is negligible in comparison to the
116 dislocation density after deformation (Table 1). Figure 1 a and b shows back-scattered electron
117 images of decorated dislocations in corresponding areas in the samples from the same pair before
118 and after annealing, respectively. c -screw dislocations appear as lines and c -edge dislocations
119 appear as dots on the (100) plane due to their geometries. A decrease in dislocation density was
120 observed by comparing the images before and after annealing. The water content in the samples
121 before and after annealing was below the detection limit of infrared spectroscopy. The transmission

electron microscope images of the dislocation structures after deformation are given in Fig. 4 in Wang et al. (2016).

Figure 1c plots the logarithmic rate constants of *c*-edge dislocation annihilation against the reciprocal temperature. The results from the previous dislocation recovery experiments on *c*-screw dislocations (Wang et al., 2016) and of other studies on dislocation recovery kinetics are also plotted in this figure. The dislocation annihilation rate constants of *c*-edge and *c*-screw dislocations are comparable, but those of the *c*-screw are about half an order of magnitude higher than those of the *c*-edge. The temperature dependences for these two dislocations are identical. Their activation energies are $E_{c\text{-edge}} = 400 \pm 20$ kJ/mol and $E_{c\text{-screw}} = 400 \pm 30$ kJ/mol for the *c*-edge and *c*-screw, respectively.

Discussion

The identical activation energies of annihilation rate constants of the *c*-edge and *c*-screw dislocations indicate that the motions of both dislocations are controlled by the same mechanism. Although many transport properties of olivine exhibit activation energies of 300 to 500 kJ/mol (e.g., Dohmen et al., 2002, 529 ± 41 kJ/mol for silicon self-diffusion, 338 ± 14 kJ/mol for oxygen self-diffusion), they are distinct from those determined in this study (see also the slope in Fig. 3 and references therein). The high accuracy of activation energies obtained in previous studies and the present one allows us to distinguish the rate-limiting mechanisms of different processes.

The motion of edge dislocations is controlled by climb at high temperatures and low stresses (e.g., Hull and Bacon, 2001; Kohlstedt, 2006). However, the motion of a pure screw dislocation does not involve climb because screw segments have no specific slip plane (Hull and Bacon, 2001).

144 Since jogs in screw dislocations have an edge character, we propose that the motion of screw
145 dislocation is controlled by the climb of jogs (Fig. 2). A screw dislocation can form a jog by
146 cross-slips to overcome obstacles that it meets during glide (Fig. 2A and 2B). The slip plane of the
147 jog is defined by its dislocation line (\mathbf{J}) and the Burgers vector (\mathbf{b}), which is indicated by the yellow
148 plane. The parent screw dislocation glides in the y direction, and therefore the jog needs to climb in
149 the y direction to move along with its parental dislocation so that the screw dislocation can go
150 through the obstacle (Fig. 2C). This climb of jogs should serve as the rate-limiting process of screw
151 dislocation motions.

152 It should be noted that although the climb of edge dislocation and jog motion of screw
153 dislocation are essentially the same, the density of climbing parts on edge dislocations and that of
154 jogs on screw dislocations may be different, creating differences in the magnitudes of rate constants.
155 Thus, only the slope in the Arrhenius plot can serve as a fingerprint of the essential mechanism of
156 rate-limiting processes in dislocation recovery experiments.

157 Since climb is controlled by diffusion, the diffusivities derived from annihilation rate constant
158 D^R (based on Karato and Ogawan, 1989) were compared with those of silicon and oxygen diffusion
159 in olivine (Fig. 3). None of these data fit D^R well. Instead, D^R falls between silicon lattice and grain
160 boundary diffusivities. This result indicates that the dislocation climb in olivine may be controlled
161 by pipe diffusion. Vacancies, dislocations and grain boundaries are 0-, 1-, and 2-dimensional defects,
162 respectively, the structure distortion near these defects should increase consequently and
163 accordingly the associated Si diffusivity should increase. In addition, the activation energy of D^R
164 obtained in this study is between those of Si lattice (540 kJ/mol, Dohmen et al., 2002) and grain
165 boundary diffusion (~200 kJ/mol, Fei et al., 2015). This result is also consistent with the hypothesis

166 that pipe diffusion controls dislocation climb (Hirth and Kohlstedt, 2015). Although there are no
167 data for pipe diffusion in olivine, the fact that the diffusion coefficient and activation energy of pipe
168 diffusion fall between those of lattice and grain boundary diffusion is well established for oxides
169 (Frost and Ashby, 1983, Table 12.1). The low activation energy of oxygen lattice diffusion (~340
170 kJ/mol, Dohmen et al., 2002) rules out the possibility that oxygen diffusion controls dislocation
171 climb.

172

173 **Implications**

174 Our results suggested that the conventional climb model can be used to dislocation motions in
175 olivine regardless of dislocation characters. Although only [001] dislocation is studied in this study,
176 the conclusion can be applied to dislocations with different Burgers vectors in olivine. The
177 cross-slip model requires the recombination of dissociated screw dislocations. If the dissociation
178 distance between two partial dislocations is large, the recombination is difficult. In this case, the
179 cross-slip of screw dislocations can be a rate-limiting process (Poirier, 1976). Previous study
180 (Vander Sande and Kohlstedt, 1976) has revealed that the dissociation distances of [001] and [100]
181 dislocation are similar (~4 nm). Therefore, cross-slip cannot be the rate-limiting process for both
182 [100] and [001] dislocations judging from present study. Although dissociation of [010] dislocations
183 has been reported (Fujino et al., 1993), its low abundance makes its effect on olivine dislocation
184 creep less important.

185 The observation that screw dislocation motion in olivine is controlled by climb of jogs
186 indicates that the softness of the asthenosphere cannot be attributed to the cross-slip controlled
187 dislocation creep of olivine (Poirier and Vergobbi, 1978). Other factors, such as melt and water,

188 could explain the softness of asthenosphere (Hirth and Kohlstedt, 2003). Although this explanation
189 is refuted by Si lattice diffusion (Fei et al., 2013), our results indicate that dislocation climb in
190 olivine is controlled by pipe rather than lattice diffusion under dry conditions. Further study on the
191 water effect on dislocation recovery could reconcile the discrepancy between deformation and
192 diffusion experiments results.

193 **Acknowledgments**

194 We thank H. Fischer and R. Njul of BGI for the sample and for assembly preparation. This
195 research was supported through DFG grants to TK (KA3434-3/1, KA3434-3/2, KA3434-7/1 and
196 KA3434-8/1) and with the annual budget of BGI. All data used in this paper are given in Table 1
197 and plotted in Fig. 1c and have been archived at Earth and Space Science Open Archive
198 doi.org/10.1002/essoar.10501470.1.

199

References

- Bai, Q., and Kohlstedt, D. L., 1992, High-temperature creep of olivine single crystals, 2. dislocation structures: *Tectonophysics*, v. 206, no. 1–2, p. 1-29.
- Becker, T. W., 2017, Superweak asthenosphere in light of upper mantle seismic anisotropy: *Geochemistry, Geophysics, Geosystems*.
- Craig, C. H., and McKenzie, D., 1986, The existence of a thin low-viscosity layer beneath the lithosphere: *Earth and Planetary Science Letters*, v. 78, no. 4, p. 420-426.
- Dohmen, R., Chakraborty, S., and Becker, H.-W. (2002) Si and O diffusion in olivine and implications for characterizing plastic flow in the mantle. *Geophysical Research Letters*, 29(21), 2030.
- Farver, J.R., and Yund, R.A. (2000) Silicon diffusion in forsterite aggregates: Implications for diffusion accommodated creep. *Geophysical Research Letters*, 27(15), 2337-2340.
- Fei, H., Koizumi, S., Sakamoto, N., Hashiguchi, M., Yurimoto, H., Marquardt, K., Miyajima, N., Yamazaki, D., and Katsura, T., 2016, New constraints on upper mantle creep mechanism inferred from silicon grain-boundary diffusion rates: *Earth and Planetary Science Letters*, v. 433, p. 350-359.
- Fei, H., Wiedenbeck, M., Yamazaki, D., and Katsura, T., 2013, Small effect of water on upper-mantle rheology based on silicon self-diffusion coefficients: *Nature*, v. 498, no. 7453, p. 213.
- Frost, H.J. and M.F. Ashby, *Deformation mechanism maps: the plasticity and creep of metals and ceramics*. 1982: Pergamon press.
- Fujino, K., H. Nakazaki, H. Momoi, S.-i. Karato, and D. L. Kohlstedt (1993), TEM observation of dissociated dislocations with $b=[010]$ in naturally deformed olivine, *Physics of the earth and planetary interiors*, 78(1-2), 131-137.
- Gose, J., Schmaedicke, E., Markowitz, M., and Beran, A., 2010, OH point defects in olivine from Pakistan: *Mineralogy and Petrology*, v. 99, no. 1-2, p. 105-111.
- Hager, B. H., 1991, Mantle viscosity: A comparison of models from postglacial rebound and from the geoid, plate driving forces, and advected heat flux, *Glacial isostasy, sea-level and mantle rheology*, Springer, p. 493-513.
- Hirth, G., and Kohlstedt, D., 2003, Rheology of the Upper Mantle and the Mantle Wedge: A View from the Experimentalists, *Inside the Subduction Factory*, American Geophysical Union, p. 83-105.
- Hirth, G., and Kohlstedt, D., 2015, The stress dependence of olivine creep rate: Implications for extrapolation of lab data and interpretation of recrystallized grain size: *Earth and Planetary Science Letters*, v. 418, p. 20-26.
- Hull, D., and Bacon, D. J., 2001, *Introduction to dislocations*, Butterworth-Heinemann. P.257
- Karato, S., and Ogawa, M., 1982, High-pressure recovery of olivine: implications for creep mechanisms and creep activation volume: *Physics of the Earth and Planetary Interiors*, v. 28, no. 2, p. 102-117.
- Karato, S., Scanning electron microscope observation of dislocations in olivine. *Physics and Chemistry of Minerals*, 1987. 14(3): p. 245-248.
- Kohlstedt, D.L., et al., New Technique for Decorating Dislocations in Olivine. *Science*, 1976. 191(4231): p. 1045-1046.

243 Kohlstedt, D., Nichols, H., and Hornack, P., 1980, The effect of pressure on the rate of dislocation
 244 recovery in olivine: *Journal of Geophysical Research: Solid Earth* (1978–2012), v. 85, no.
 245 B6, p. 3122-3130.
 246

247 Kohlstedt, D. L., 2006, The Role of Water in High-Temperature Rock Deformation: Reviews in
 248 Mineralogy and Geochemistry, v. 62, no. 1, p. 377-396.

249 Kohlstedt, D. L., and Goetze, C., 1974, Low-stress high-temperature creep in olivine single crystals:
 250 *Journal of Geophysical Research*, v. 79, no. 14, p. 2045-2051.

251 Mackwell, S.J., Kohlstedt, D.L., and Paterson, M.S. (1985) The role of water in the deformation of
 252 olivine single-crystals. *Journal of Geophysical Research-Solid Earth and Planets*, 90(NB13),
 253 1319-1333. Peltier, W., 1998, Postglacial variations in the level of the sea: Implications for
 254 climate dynamics and solid - earth geophysics: *Reviews of Geophysics*, v. 36, no. 4, p.
 255 603-689.

256 Poirier, J. (1976), On the symmetrical role of cross-slip of screw dislocations and climb of edge
 257 dislocations as recovery processes controlling high-temperature creep, *Revue de Physique*
 258 *Appliquée*, 11(6), 731-738.

259 Poirier, J.-P., 1985, Creep of crystals: high-temperature deformation processes in metals, ceramics
 260 and minerals, Cambridge University Press.

261 Poirier, J.-P., and Vergobbi, B., 1978, Splitting of dislocations in olivine, cross-slip-controlled creep
 262 and mantle rheology: *Physics of the Earth and Planetary Interiors*, v. 16, no. 4, p. 370-378.

263 Vander Sande, J., and D. Kohlstedt (1976), Observation of dissociated dislocations in deformed
 264 olivine, *Philosophical Magazine*, 34(4), 653-658.

265 Wang, L., Blaha, S., Pintér, Z., Farla, R., Kawazoe, T., Miyajima, N., Michibayashi, K., and Katsura,
 266 T., 2016, Temperature dependence of [100](010) and [001](010) dislocation mobility in
 267 natural olivine: *Earth and Planetary Science Letters*, v. 441, p. 81-90.

268 Weertman, J., 1955, Theory of Steady - State Creep Based on Dislocation Climb: *Journal of*
 269 *Applied Physics*, v. 26, no. 10, p. 1213-1217.
 270

Figure and table captions

Figure 1. BEIs showing the dislocation density (a) before and (b) after annealing at 1760 K for 35 min. The images were taken on the (100) plane. Screw and edge dislocations are shown as lines and dots, respectively, due to the geometries of their dislocation lines. The yellow scale bar denotes 2 μm . (c) Logarithmic dislocation annihilation rate constants of c -edge dislocations versus reciprocal temperature. The annihilation rate constants of c -screw dislocations from Wang et al. (2016) are plotted together. The activation energies for both dislocations are identical, i.e., 400 kJ/mol. Previous results on dislocation recovery are also plotted for comparison.

Figure 2. A schematic diagram showing the jog-climb controlled motion of a screw dislocation. (a) The screw dislocation (blue line) is elongated in the x direction, which is parallel to its Burgers vector \mathbf{b} , and glides in the y direction. The blue dot represents the obstacle that the screw dislocation meets during glide. (b) A jog (red segment) elongated in the z direction is produced on the screw dislocation to overcome the obstacle. This jog has an edge nature with the same Burgers vector \mathbf{b} as that of the parental screw dislocation. The yellow area indicates the glide plane of the jog, which is normal to the y direction. (c) The jog has to climb out of its glide plane to move along with its parental screw dislocation.

Figure 3. Logarithmic diffusivity derived from dislocation annihilation rate constants of c -edge and c -screw dislocations versus reciprocal temperature. Si and O lattice and grain boundary diffusivities are plotted together.

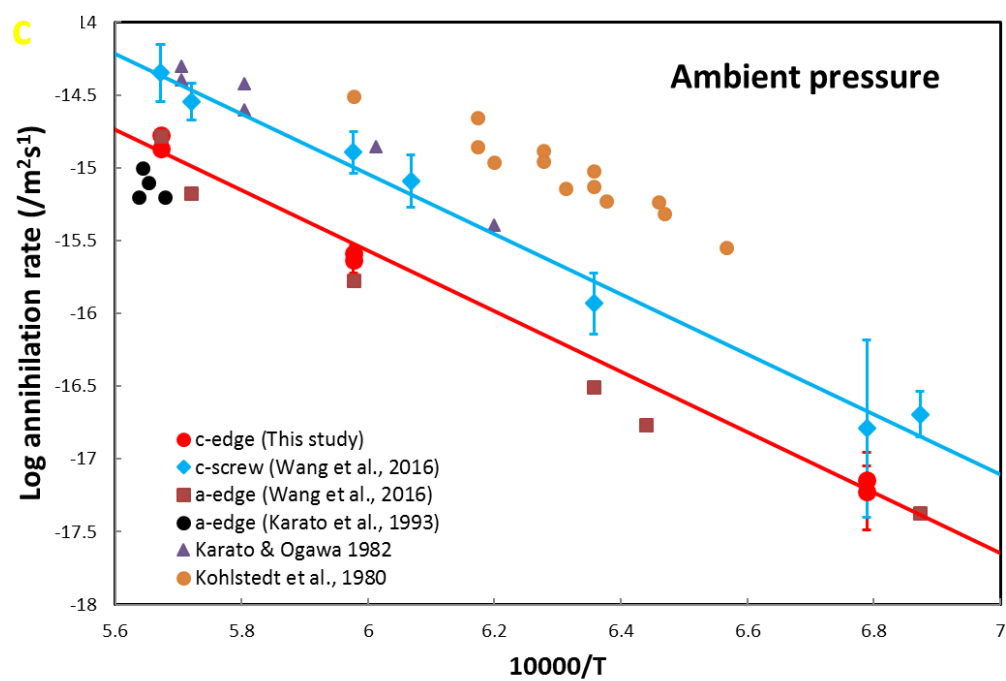
Table 1. Summary of the experimental conditions and results.

Table 1. Summary of the experimental conditions and results*.

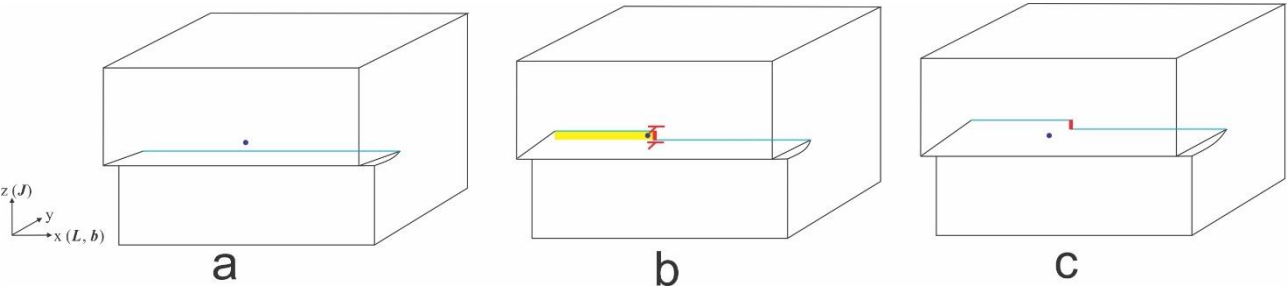
[001](010) edge dislocation						
Sample	T (K)	Annealing time (h)	$\log(f_{o_2}, 10^5 \text{ Pa})$	$\rho_i (\mu\text{m}^{-2})$	$\rho_f (\mu\text{m}^{-2})$	$\log(k, \text{m}^2\text{s}^{-1})$
Z1643-1	1763	0.58	-4.9	1.60±0.13	0.29±0.01	-14.87±0.03
				0.97±0.13	0.22±0.01	-14.77±0.03
Z1643-2	1673	2.5	-5.7	1.49±0.04	0.36±0.06	-15.63±0.09
				1.13±0.12	0.31±0.03	-15.58±0.05
Z1643-3	1473	24	-7.7	1.33±0.15	0.73±0.05	-17.14±0.09
				0.35±0.03	0.29±0.01	-17.22±0.27

* different ρ_i and ρ_f values of each sample correspond to different areas

301



306 Figure 2.



307
308

